Groundwater fluxes and flow paths within coastal barriers: Observations from a large-scale laboratory experiment (BARDEX II)

Turner, I.L.; Rau, G.C.; Austin, M.J.; Andersen, M.S.

Coastal Engineering

DOI:
10.1016/j.coastaleng.2015.08.004

Published: 01/07/2016

Peer reviewed version

Groundwater fluxes and flow paths within coastal barriers: observations from a large-scale laboratory experiment (BARDEX II)

Ian L. Turner[a*], Gabriel C. Rau[a,b], Martin J. Austin[c] and Martin S. Andersen[a,b]

[a] *Water Research Laboratory, School of Civil and Environmental Engineering, UNSW Australia, Sydney, NSW 2052, Australia*

[b] *Connected Waters Initiative Research Centre, UNSW Australia, Sydney, NSW 2052, Australia. Affiliated with the National Centre for Groundwater Research and Training, Australia.*

[c] *School of Ocean Sciences, Bangor University, Menai Bridge, Anglesey LL59 5AB, UK*

[*]corresponding author: *ian.turner@unsw.edu.au*

REVISED JULY 2015

Submission to: COASTAL ENGINEERING (BARDEX II Special Issue)

ABSTRACT

The dynamics of groundwater at the beach face land-ocean boundary have important implications to the exchange of water, nutrients and pollutants between the ocean and coastal aquifers, and more subtly, varying groundwater levels may induce differing morphological response at the beach face. As a component of the multi-institution Barrier Dynamics Experiment (BARDEX II), groundwater fluxes and flow paths within a prototype-scale sandy barrier are quantified and reported at the three fundamental spatio-temporal scales (individual waves, the beach face and total barrier), under controlled wave and water-level conditions. A particular feature of the experimental program was the inclusion of a back-barrier 'lagoon', that via a pump system and an intermediate water reservoir enabled the forcing of contrasting hydraulic gradients across the barrier. It was observed that the groundwater level, flow paths and fluxes within the beach face region of the sand barrier were predominantly controlled by the action of waves at the beach face, regardless of the overall seaward- or landward- directed barrier-scale hydraulic gradients. In the presence of waves all tests undertaken to complete this study developed a seaward gradient in this zone under the influence of waves. As a further result of wave forcing at the beach face boundary, localised groundwater flow divides were observed to develop, further partitioning the circulation and flow paths of groundwater within the prototype scale sand barrier.

1 INTRODUCTION

The dynamics of groundwater at the beach face land-ocean boundary have important implications to the exchange of water, nutrients and pollutants between the ocean and coastal aquifers (e.g., Robinson et al., 2006; Andersen et al., 2007; Anschutz et al. 2009), and more subtly, varying groundwater levels may induce differing morphological response (erosion versus accretion) at the beach face (e.g., Turner and Masselink, 1998; Masselink and Puleo, 2006). Insight to the varying rates and direction of groundwater flow at coastal barriers is therefore of interest to a range of disciplines, including coastal engineers, hydrogeologists and ecologists. However, variable climatic and marine conditions (storms, tides, recharge, etc.) and the largely unknown geological heterogeneity of natural coastal aquifers make it very challenging at best to quantify fluid fluxes and their dynamic drivers. Large-scale laboratory experiments offer the advantage of eliminating the geological heterogeneity while the barrier hydraulic gradients and the dynamic wave conditions can be varied systematically to reveal how these variables affect specific aspects of coastal barrier hydrology (e.g., Turner and Masselink, 2012).

As a component of the multi-institution Barrier Dynamics Experiment (BARDEX II), groundwater fluxes and flow paths at three spatio-temporal scales were observed and quantified under controlled wave and water-level conditions within a prototype-scale sandy barrier. This work was undertaken as one of six Work Packages completed during the period May to July 2012 in the Delta Wave Flume, The Netherlands. The specific objectives, coordination of individual work packages and details of all instrumentation deployed by the BARDEX II Project Team are detailed in Masselink et al., (this volume). In total, more than 30 personnel from 6 countries representing 8 research institutions in Europe, the USA and Australia worked together for a total of 20 experimental days (58 days from commencement to decommissioning) to complete the full test program. Provided here is an overview of the experimental set-up and instrumentation relevant to the Work Package 1 ‘Barrier

Hydrology' objectives of the research program. The outcomes of the other five Work Packages are reported elsewhere in this volume.

The specific focus of the work presented here is to provide an overview of the direction and magnitude of observed groundwater fluxes within the prototype-scale sand barrier at three contrasting spatio-temporal scales: (1) instantaneous in/exfiltration across the swash zone forced by the runup-backwash of individual waves; (2) time-averaged groundwater flow distribution beneath the groundwater mound at the beach face induced by the presence of waves; and (3) water table profiles and resulting net groundwater fluxes through the entire barrier. The three spatio-temporal scales were investigated for high versus low lagoon levels, and in the presence/absence of wave action at the seaward side of the barrier. In the following Section 2 an overview of the laboratory experiment and specific barrier hydrology instrumentation is provided, with the reader referred to Masselink et al (this volume) for full details of the BARDEX II experimental design, instrumentation and test program. The results presented in Section 3 separately describe and quantify groundwater fluxes at these three scales of interest. Section 4 then provides a discussion and synthesis of these observations, to characterise and contrast the differing space- and time-scales of groundwater flow paths and fluxes within sandy coastal barriers, and to elucidate the relative importance of wave action versus barrier-scale hydraulics gradients.

2 METHODOLOGY – BARDEX II TEST PROGRAM AND GROUNDWATER INSTRUMENTATION

2.1 Overview

A key feature of the BARDEX II test program was the installation of a 'lagoon' water body at the landward side of the sand barrier. By the operation of a multi-stage pump system and a third intermediate water reservoir, the water levels within the wave flume at the 'sea' (waves) and lagoon (no waves) sides of the sand barrier were separately and independently controlled and manipulated (see Masselink et al. this volume). This approach was similarly implemented during the BARDEX gravel barrier test program completed in 2008 within the same laboratory facility (Williams et al.,

2012). By this approach, lagoon levels at the landward side of the barrier were raised and lowered relative to the sea, in order to force differing hydraulic gradients across the barrier. A series of tests were undertaken to examine and contrast the effects of varying incident wave conditions at the beach face. The confounding effect of variable-density interactions (i.e., fresh-salt water) within the barrier (e.g. Bakhtyar, et al. 2012) was not considered in this experimental program where only freshwater was used in the Delta Flume. This enabled the present work to explicitly and separately examine the relative significance of waves and varying back-barrier groundwater levels to resulting barrier groundwater conditions. Further, these idealised experimental conditions also eliminated the difficult task of establishing the distribution of fresh and saline water in the barrier and the need to correct hydraulic heads for variable density effects (Acworth, 2007; Post and von Asmuth, 2013).

2.2 Sand barrier characteristics and lagoon–sea pump system

A 4.5 m high, 5 m wide and 100 m long sand barrier composed of medium-sized sand (*D50* = 0.42 mm; *D10* = 0.26 mm; *D90* = 0.90 mm) was constructed with the initial barrier crest located at around 110 m from the front face of the wave paddle, within the 250 m long, 5 m wide and 7 m deep Delta Wave Flume (Figure 1). In all figures and text, the origin of the coordinate system is located at the front face of the rest position of the wave paddle (x = 0 m) at the elevation of the wave flume floor (z = 0 m). The sand grain size distribution and the resulting barrier permeability and porosity characteristics (refer Section 2.4) were somewhat lower than was originally planned, and as a result there was evidence that steady state groundwater conditions were not completely achieved during and between every test completed, due to the long duration of flow times required for the groundwater profile within the central region of the barrier to reach a new steady state in response to varying lagoon level and wave conditions. Note is made below where this occurred.

Referring to Figure 1, a concrete toe (located at x = 24-29 m) followed by a 20 m wide and 0.5 m deep horizontal sand bed, fronted the main 60 m wide, seaward sloping (1:15) section of the sand barrier (x = 49-109 m). This sloping section was topped by a 4.5 m high and 5 m wide barrier crest (x = 109-114 m), resulting in a total aquifer thickness at the beach face in the range of 3 - 4 m,

underlain by the impermeable flume floor. The 1:5 landward-sloping back barrier (114-124 m) termined with a 1 m thick and highly permeable vertical wall constructed using a 5 cm square steel mesh wrapped in a 180 micron geotextile fabric, prevented the ingress of barrier sand to the 10 m wide lagoon (x = 125-135 m). The remaining section of the Delta Flume was separated from the lagoon by a steel gate, providing a third intermediate reservoir for water pumped between the sea and lagoon sides of the sand barrier.

Four computer-controlled pumps, with a maximum pumping rate of 0.1 m^3/s, were used to regulate all water-levels in the Delta Flume, with pump discharge logged continuously. Unfortunately, once the barrier was constructed and the flume filled, it became apparent that the gate between the lagoon and reservoir sections of the flume leaked by a significant but unknown quantity. Net groundwater fluxes through the barrier could therefore not be monitored via this pump system as was originally envisaged. However, the continuous measurement of groundwater profiles through the barrier does enable these quantities to be modelled and estimated.

The complete experimental program spanning all six Work Packages comprised 6 distinct test series. Each of the test series A – F consisted of either a constant or varying lagoon and sea water-levels imposed across the barrier, which was then subjected to a range of differing wave conditions. The focus of the work presented here represents a subset of the test program comprising the first test series A, during which the water level on the sea side of the barrier (h_s) was maintained at a constant 3.0 m, and the lagoon water-level (h_l) maintained at either a raised (4.3 m) or lowered (1.75 m) elevation. Table 1 summarises the water-level and wave conditions during test series A. For the three cases of lagoon > sea (A2), lagoon < sea (A4) and lagoon = sea (A6), two irregular wave cases of H_s = 0.8 m, T_p = 8 s (A2 and A4) and H_s = 0.6 m, T_p = 12 s (A6) were run. For these irregular wave cases the wave paddle steering signal was a JONSWAP spectrum specified by H_s,T_p with a peak-enhancement factor of 3.3. The Delta Flume's Automated Reflection Compensator (ARC) was deployed at all time to avoid seiching in the flume. To enable comparison between different tests within the same test series, for tests with the same wave forcing (H_s and T_p) the identical wave

steering signal was used. In addition, at the end of each irregular waves test a shorter duration package of monochromatic then bi-chromatic waves of corresponding wave height and period (H_s = 0.8 m, T_p = 8 s; H_s = 0.6 m, T_p = 12 s) completed each of the A-series experiments. The reader is referred to Masselink et al. (this volume) for a full description of the complete test program.

To illustrate the general test procedure used on the complete series A, Figure 2 depicts the groundwater levels obtained during test A4 (lowered lagoon; refer to Table 1), with the blue colours in this figure corresponding to wells on the seaward side of the barrier, whereas red colours correspond to wells located towards the lagoon. Periods of wave actions are seen in Figure 2 as periods of elevated and fluctuating water levels towards the seaward side of the barrier. The wave action was halted for a period of 15-30 minutes at various intervals ranging from every 10 minutes to hourly, to enable the recording of a complete detailed beach profile and adjustment of instrumentation (for details refer Masselink et al., this volume). As a result, this prevented attainment of complete hydraulic steady-state throughout the barrier. For this reason, two 'characteristic' time periods (indicated in Figure 2) were used throughout the analysis presented below to assess 'wave' and 'no wave' conditions, while maximising the likelihood of conditions close to steady-state. To determine the time-average initial and final water table profile through the barrier for all A-series tests, the first time period was selected immediately prior to the onset of the first set of irregular waves, and the second time period coincided with the final minutes of irregular waves for each day of testing. It can be seen in Figure 2 that, following the final period of irregular wave testing, two additional packages of waves were also generated within the wave flume; the first was a 5 minutes sequence of mono-chromatic waves, and the second a 15 minute sequence of bi-chromatic waves. Neither of these wave conditions were used for the work reported here. Further details are described and illustrated in Section 3.

2.3 Barrier Hydrology Instrumentation

Groundwater Wells

An array of 15 groundwater wells were installed along the length of the sand barrier (Figure 1) adjacent to the flume wall, spaced at 3 m cross-shore intervals through the beach face section, then 4 m and 5 m spacing seaward and landward of this region respectively. Wells were constructed of 30 mm diameter PVC pipe, capped at the bottom and fully screened (machine-slotted and wrapped in a geotextile sock) from their base at an elevation of z = 1 m (relative to the flume floor), to an elevation 0.5 m beneath the local sand barrier surface.

Unvented pressure sensors (Kulite HKM-134) were installed at the base of each well, and centrally logged at 20 Hz throughout all test series. Atmospheric pressure was measured by a barometric pressure sensor located in a bottom-capped and water-tight well located at the barrier crest. Data from the unvented pressure sensors were subsequently corrected to determine the phreatic surface ('water table') within the barrier.

Piezometers

A set of four pairs of nested piezometers (Figure 1) were installed around the intersection of the mean sea level (z = 3.0 m) and sand barrier, to observe the vertical structure of groundwater flow beneath this active region of uprush-backwash swash flows across the beach face. Piezometers were constructed of solid and uncapped 30 mm diameter PVC pipe and located adjacent to the flume wall. The open base of the lower piezometer pair were all installed at an elevation of z = 0.5 m relative to the flume floor, with the open base of the upper piezometer for each pair located at z = 2.5 m. Again, unvented pressure transducers (Solinst Levelogger Edge) were fixed within each piezometer, logged at 1 Hz and corrected for local atmospheric pressure variation.

Buried PTs

Two vertical arrays of high-precision (Druck PTX1830HR) unvented pressure transducers (PTs henceforth), each comprised of three, were buried directly into the beach face to measure vertical pressure gradients. To exclude sand grains from directly impacting the sensing diaphragm, the sensing ports of the PTs were wrapped in 250 micron geotextile fabric. The PTs were mounted on a

thin stainless steel rod, with the sensing ports pointing upwards. The vertical distance between the sensors was fixed at 100 mm. The arrays were buried into the beach face, with the diaphragm of the upper PT nominally 6 cm below the sand surface. The elevation of the PTs were adjusted between each period of wave action to maintain this consistent depth of burial relative to the beach face surface, where measureable bed-level change was observed. An additional identical PT was used to sample atmospheric pressure, to again enable correction for local atmospheric pressure variation. These PTs were cabled to a time-synchronised data-logger and sampled at 20 Hz.

Referring to the location of these direct burial PTs as indicated in Figure 1, one array (PT1) was typically deployed just landward of the still water level in the mid-swash region, while the position of the more landward second array (PT2) was varied for individual tests to measure vertical pressure gradients at different relative positions across the swash zone. Array PT1 was thus generally inundated by each swash event, whereas array PT2 was typically only inundated by the largest swashes.

Solute Groundwater Tracing

Direct barrier pore water flow rates were determined at two sites by monitoring the physical transport of a solute tracer (a solution of NaCl) introduced into the barrier sand. Cubic stainless steel frames (0.5 × 0.5 × 0.5 m) were constructed to provide rigid mechanical support for fixing two tracer source pipes as well as fluid electrical conductivity (EC) sensors for measuring the tracer migration. A total of 2 rigs were installed for solute tracing. One rig was buried below the surface at the swash zone (x = 90.26 m, y = 2.23 m) and referred to as the Swash-rig, the other was buried further into the barrier (x = 98.96 m, y = 2.07 m) and referred to as the Barrier-rig.

For each solute rig two vertical solute source pipes were constructed of 30 mm diameter PVC pipes screened over 1 m and extended by solid pipe to above the beach face for access (see Figure 3). These pipes were mounted at each end of the rigs in the cross-shore direction 0.5 m apart. In between them, 5 micro-EC sensors (Microelectrodes Inc., USA) were mounted at different distances.

Solute slugs were introduced into the source pipes by a feeder tube which was constructed from a Perspex pipe having a slightly smaller diameter allowing it to fit inside the access pipes. The feeder tube had a rubber plug at the lower end that could be removed by pulling a string from the top. The feeder tube enabled controlled release of dilute solute slugs by lowering it to the bottom of the source tubes. Then the rubber plug was pulled and the feeder tube was slowly and evenly lifted up to leave an even vertical salt slug in the source pipe. The salt slug would then migrate through the screened section of the pipe into the barrier with the ambient hydraulic gradient. The NaCl concentration of the salt slugs was kept below an equivalent EC of 6,000 µS/cm (at 20 °C) to minimise density effects in the source pipe. The slug transport was tracked by the EC sensors on the surrounding steel-frame rig (Figure 3). A PC-based control system was simultaneously logging the 12 channels of fluid electric conductivity (EC) at 1 Hz sampling frequency (see Rau et al., 2012 for further details).

2.4 Barrier Hydraulic Properties

Representative samples of the barrier sand were analysed for porosity and hydraulic conductivity. These properties are required to quantify the fluxes through the barrier using water levels and solute tracer tests. The porosity was calculated using the bulk dry and wet density of a representative sample. The sand was fully saturated by wet-packing, and the volumes as well as weights of the sample were measured with a volumetric glass cylinder and a laboratory-grade scale. The sample was then oven dried at 110 °C and the density analysis was repeated. The difference in wet and dry density is directly proportional to the porosity of the sample, here determined as 41%.

The hydraulic conductivity (K) of sand samples was estimated by a series of constant head tests. The sand was wet-packed into a vertical column of known dimensions. Constant flows at different rates were then induced through the column and the pressure difference was measured using a manometer board. A total of 20 constant flux tests on 3 different samples provided an average value of 8×10^{-4} m/s ± 1×10^{-4} m/s. This value in combination with porosity and the water level

measurements was used to quantify groundwater flow rates and fluxes through the barrier using Darcy's law (refer below).

2.5 Barrier Hydrology Data Processing and Analysis

Quantification of instantaneous vertical fluxes

Instantaneous vertical fluxes (*w*) through the beach face were determined in the swash zone via the vertical pressure gradient between the two uppermost buried PTs in the vertical arrays PT1 and PT2 using Darcy's law for flow in porous media:

$$w = -K\frac{dp}{dz} \quad (1)$$

where *K* is hydraulic conductivity and *dp/dz* the local vertical pressure gradient. Data were corrected for barometric pressure variations and the pore-pressure difference between the upper and lower sensors *dp* was computed by subtracting the hydrostatic pressure offset $P_{off} = \rho g dz$ between the upper and lower sensors, where ρ is the fluid density, *g* gravity, *dz* the vertical sensor separation. Using Eq. (1), the dimensionless parameter w/K and hence w, were modelled.

The vertical fluxes were quantified during a period with waves within each test series where quasi-steady-state for the overall barrier hydraulic gradients was obtained. For each case the pressure gradients were analysed over the same 180 s period at the end of the longest irregular wave run in each test series.

Quantification of the barrier flow field

Flows within and through the barrier were quantified within each test series for a hydraulic steady-state without waves (before the waves were switched on) and for a hydraulic quasi-steady-state with waves (at the end of the final irregular wave run within each test). For each case the hydraulic heads measured in each well were averaged over a 5 minute time period representative of the above conditions. In order to quantify the through-barrier flows the 2D head distribution within the barrier was derived as follows: A mesh grid consisting of variably sized triangles with sides approx.

0.1 m in length was constructed for the water saturated part of the barrier for each 300 s time period. This domain extended horizontally from the first well (x = 75 m) to the lagoon (x = 124 m) with vertical side boundaries. The top boundary of the domain was determined by either the measured barrier profile elevation when submerged (by the sea or lagoon) or the water table in the barrier (for the part of the barrier not submerged). The resulting triangular mesh consisted of approx. 800-1000 elements depending on test series and conditions. The *Laplace* equation was solved using 2D finite element analysis with the following boundaries: no-flow (*Neumann*) boundary condition at the bottom, constant head (*Dirichlet*) boundary condition along all other sides as derived from the pressure loggers. Using the calculated hydraulic heads the horizontal and vertical hydraulic gradient distribution was interpolated for a 2D grid with uniform spacing of 0.05 m across the domain.

The calculated hydraulic head distributions were used to construct equipotential contours and flow lines in order to visualise the flow field. It should be noted that these flow lines do not imply total particle pathways, but rather represent an instantaneous picture of flow vectors. The horizontal component of the gradient field was used to quantify the flow through the barrier at both the intersection with the sea and the lagoon.

Quantification of water movement from tracer transport

While flow rates derived from hydraulic gradients are subject to uncertainty in the estimation of the hydraulic conductivity, solute tracers provide a direct measurement of water movement through the sand. An injected conservative solute tracer is transported through with the moving water. The cumulative concentration of a solute slug passing an EC-sensor located at a discrete point in space can be expressed as a tracer breakthrough curve. Normalised integrated EC tracer breakthrough curves were derived from the measured EC pulses. These represent the cumulative mass of the tracer slug as it moves past each sensor. By determining the time when 50% of the slug mass has passed between 2 sensors and knowing the travel distance as well as material porosity a robust estimate of the barrier flow velocity can be calculated (Wakao and Kagei, 1982; Rau et al., 2012).

3 RESULTS

Presented in this section are the key results that were obtained to characterise and quantify the fluxes and flow paths of groundwater within the BARDEX II sand barrier at the three contrasting spatio-temporal scales investigated. The order of presentation is from the largest to the smallest (both in time and space); starting with the observation of characteristic groundwater mounding across the entire barrier profile, to the time-average groundwater circulation that this mounding induces beneath the beach face, to finally the resulting instantaneous infiltration/exfiltration forced by individual swash across the beach face. At all three space/time-scales considered, the influence of a raised versus lowered lagoon level at the back of the barrier is explicitly identified.

3.1 Through-barrier water table profiles, flow paths and fluxes

The water table profiles across the full extent of the BARDEX II sand barrier subject to the differing lagoon levels and wave conditions listed in Table 1 were quantified by the array of 15 groundwater wells installed along the length of the sand barrier. As these wells were slotted over the full saturated depth, the measurement of the vertical head within each well equates to the local height of the phreatic surface (or water table) in the adjacent barrier sand (for further explanation of the differing coastal groundwater applications of slotted wells versus non-slotted piezometers, refer Turner, 1998). Figure 4 shows the water table profiles and equipotential lines for the three cases of A6 sea=lagoon (Figure 4a), A2 raised lagoon water level (Figure 4b) and A4 lowered lagoon level (Figure 4c), for test conditions with and without waves. Also shown in these figures are calculated flow paths based on trajectories orthogonally to the equipotential lines (please note these are instantaneous flow trajectories rather than actual travel paths). In the case of A6; sea level equal to lagoon level without waves, there is a small rise in the water table under the beach face. Retrospectively it became apparent that the water table was still re-equilibrating following the previous day's experimentation. For conditions with waves the final water table elevations through the cross-shore transect of wells is derived for the final 300 seconds of irregular waves. Due to the

damping effects of the 30 mm fully-slotted wells, short-term fluctuations of the phreatic surface within each well were barely discernible from the mean profile.

Once the irregular waves have been running for some time a groundwater mound (and hence a local groundwater divide) developed beneath the beach face, due to infiltration of 'sea' water in the swash zone. This characteristic feature of water table over-height in the vicinity of the beach face is previously reported by numerous authors (e.g., Kang et al., 1994, Turner et al., 1996, Sous et al., 2013). Nielsen (2009) provides a comprehensive synthesis of a range of experimental research that has examined the quasi-steady over-height of the water table adjacent to the coast caused by waves. For further discussion and recent insight to the water table over-height phenomenon that extends the analysis to gravel barriers and varying back-barrier groundwater conditions, the reader is referred to Turner and Masselink (2012).

The development of a groundwater divide was observed irrespective of the relative sea and lagoon levels. This means that for all cases in the presence of wave action, a local flux of infiltrated 'sea' water was directed back towards the sea regardless of the net through-barrier hydraulic gradient. For the cases of sea = lagoon and sea > lagoon a significant flux of infiltrated water was also directed towards the lagoon. Total net through-barrier fluxes were calculated at the two cross-sections (shown in Figure 4) where the barrier intersect the sea and the lagoon respectively, and are summarised in Table 2. The fluxes at the beach face increase with the presence of waves, due to the steepening gradients caused by the localised water table mounding. This creates a flow cell circulating significant amounts of infiltrated seawater back into the sea. Interestingly the seaward flux at the beach face (Table 2) has no correlation to the water level in the lagoon as one would expect, but is entirely controlled by the groundwater gradient in the beach face and the sea level.

The total through-barrier fluxes were modelled by Darcy calculations using the net hydraulic gradients, the saturated cross-sectional area at the seaward and lagoon side of the barrier, and the hydraulic conductivity determined by the constant head tests. As an independent check on these fluxes solute tracer data from the tracer rigs (Figure 3) were used for test case A2 without waves

(background flow) to calculate the groundwater flow velocity at the two rig locations within the barrier (see Figure 1 for locations). Figure 5 shows individual breakthrough curves for both rigs and test series A2 without waves. Unfortunately, the centre EC sensor of the swash rig did not produce meaningful measurements, and due to its deep burial within the barrier, could not be rectified. The swash rig recorded a Darcy velocity of 3.2 m/d ± 0.13 m/d (based on the uncertainty in sensor spacing), whereas the groundwater velocity was slower at the barrier rig with an average of 2.5 m/d ± 0.11 m/d. By knowing the saturated thickness at these two sites, these Darcy velocities can be converted into total fluxes giving 5.6×10^{-4} m^3/s at the swash rig and 5.2×10^{-4} m^3/s at the barrier rig. This is within a factor of 2-3 of the values for A2 without waves (Table 2), which in the field of experimental hydrogeology is very close agreement, and confirms the general reliability of both flux estimates.

3.2 Groundwater flow beneath the beach face

The groundwater flow field beneath the beach face is a function of the forcing hydraulic processes at different spatial and temporal scales, i.e. localised infiltration/exfiltration through the beach face surface and to a lesser degree the overall background hydraulic gradient. Based on data from the point piezometers below the beach, Figures 6a-c contrast the time-averaged hydraulic head distributions within the beach face with and without the action of wave run-up, for the three cases of sea=lagoon (Figure 6a), raised lagoon water level (Figure 6b) and lowered lagoon level (Figure 6c). Referring to the upper panel in each of these three figures, the overall flow field beneath the beach face in the absence of wave action is shown for representative test series: A6 (equal sea and lagoon level), A2 (lagoon level higher than sea level), and A4 (sea level higher than lagoon level). Refer to Table 1 for specific test details. A small seaward flux was observed in test series A6 (Figure 6a) before the waves were turned on despite the intention of having no hydraulic gradient in the barrier. As noted earlier in section 3.2 this small flux is an artefact of the barrier not yet having reached equilibrium from adjustment of water levels in-between the tests. As anticipated, Figures 6b&c clearly illustrate that the flow field for the case of no waves beneath the beach face is

dominated by the sea/lagoon hydraulic gradients (i.e., high versus low lagoon levels). It is apparent that the fluxes are predominantly horizontal, with directions reflecting the overall hydraulic gradient within the barrier. However, a component of upward and downward flow can be observed for seaward and landward gradients, respectively.

The lower panels in Figures 6a-c show the flow field developed beneath the beach face as a result of the irregular wave forcing. Calculated for data at the end of each test series, these cases represent a quasi-steady-state for the hydraulic gradients in the barrier, but with a transient wave-drive hydraulic boundary at the seaward side. In contrast to the cases without waves, the flow field is now dominated by horizontal gradients in the seaward direction for all combinations of sea and lagoon levels. This means that irrespective of the overall barrier gradients (between sea and lagoon) a localised net circulation cell is established within in the beach face with infiltration in the wave run-up zone and exfiltration further seaward. Table 3 quantifies the horizontal and vertical components of these local fluxes (derived from hydraulic gradients and the hydraulic conductivity estimates) through the circulation area. The net horizontal flux component is in the range of 2.51×10^{-5} to 3.25×10^{-5} $m^3/s/m$, whereas the net vertical flux is an order of magnitude less than this, in the range of 1.69×10^{-6} to 3.64×10^{-6} $m^3/s/m$. Note that instantaneous and rapidly-reversing vertical fluxes associated with individual runup events (i.e., swash in/exfiltration) are much greater than this (refer next section). It is interesting to note that both series A6 (zero through-barrier gradient) and A4 (landward gradient) show higher horizontal fluxes towards the sea than series A2 (seaward gradient). The primary explanation is that the much larger local hydraulic gradients within the beach face are principally driven by the waves and swash run-up and associated infiltration. Within the beach face, this completely dominates over the magnitude and direction of the background hydraulic gradients caused by the relative difference in the sea and lagoon levels.

3.3 Instantaneous swash infiltration-exfiltration

It is evident from the results presented above that the instantaneous vertical flux through the beach face of a portion of the swash lens that occurs at the time-scale of individual waves, is the key process responsible for modifying the time-averaged groundwater flow and barrier water table profile, by transferring fluid volume between the surface and subsurface domains. The key factor to consider when quantifying the vertical flux in the swash zone is the location of sensors relative to the seepage face. This is a function of sea level and the characteristics of wave run-up.

Test Series A2 (high lagoon) and A4 (low lagoon) were selected here to provide a comparison between the instantaneous through-bed fluxes under opposing barrier-scale hydraulic gradients (Figures 7a&b). The instantaneous pressure data from the more seaward PT1 for both tests (refer locations in Figure 6) are used for illustration here, and are very similar for both tests. The arrival of a swash on the beach face caused a near-instantaneous increase in pore pressure at both the upper and lower sensors. The pressure difference *dp* between the vertically stacked sensors revealed a large positive pressure difference during the uprush phase of the swash event and a smaller, but longer duration negative difference during the backwash. The dimensionless parameter $-w/K$ qualifies these pressure differences as strong infiltration events during uprush and less intense but longer duration exfiltration events during backwash, with vertical velocities $w\ O(10^{-4}$ m/s).

The net average vertical discharge Q across the beach face boundary over the representative 300 s period, was computed by multiplying w by the horizontal cross-sectional area A of the flux at the sensor location (=0.05 m^2; the width of the PT pressure port 0.01 m, multiplied by the width of the flume 5 m). Exfiltration was the dominant process for both tests, but discharge during A2 (Q = 1.4 x 10^{-6} m^3/s) was an order of magnitude larger than during A4 (Q = 4.4 x 10^{-7} m^3/s). Observations of the instantaneous fluxes were also made during Test Series A6 (sea = lagoon), and A7 (high lagoon). Irrespective of the lagoon level relative to the sea, comparable rates of net infiltration were measured for both A6 (Q = -1.3 x 10^{-7} m^3/s) and A7 (Q = -1.1 x 10^{-7} m^3/s) test conditions.

Importantly, the relative position of the vertical arrays PT1 and PT2 within the swash zone was observed to determine the net direction of the instantaneous flux, with locations further landwards in the swash tending towards net infiltration. Figure 8 compares discharge at two locations during Test Series A2; array PT1 is located seaward with a relative position in the run-up of $R_{\%}$ = 60%, and PT2 further landward, with a relative position of $R_{\%}$ = 50%. Net exfiltration was observed at the more seaward PT1, while the landward PT2 revealed net infiltration, but only half the total volume of array PT1. It is noteworthy that the largest swash events (i.e. T = 80 s and 105 s) promoted events of significant instantaneous infiltration at the location PT1 compared to a background tendency for net exfiltration. The generalised observation that net infiltration predominates in the upper swash zone, in contrast to net exfiltration across the lower beach face, confirms the results of numerical simulation presented in Bakhtyar et al. (2011) and match the experimental results of Solus et al. (2013).

Figure 9 compares the net vertical flux to: (1) the relative swash zone position of each sensor array in terms of the run-up exceedance level; and (2) the barrier discharge at the ocean-barrier interface, for steady-state wave conditions during all available A series tests. There is a weak but never-the-less generally consistent relationship between the cross-shore position of the swash zone PT arrays and the net vertical flux recorded. Infiltration generally occurs at locations towards the upper-swash and exfiltration in the lower-swash. The cross-over location appears to occur at around the $R_{55\%}$ exceedance level. A stronger relationship is observed with net barrier discharge measured at the ocean-barrier interface, with infiltration generally being observed under conditions when seaward-directed discharge is stronger. The comparison of the net vertical fluxes with the fluxes in the subsurface of the beach face (Figure 6 and Table 3) and the total through barrier fluxes (Figure 4 and Table 2) is difficult, since the vertical net flux measurements are extremely sensitive to the cross-shore location of the arrays. However, from a continuity viewpoint, assuming quasi-steady state, a strong seaward discharge would have to be linked to high rates of infiltration in the upper swash zone and consequently high rates of exfiltration in the lower swash zone.

4 DISCUSSION AND SYNTHESIS

A primary observation of this experimental study is that the groundwater level, flow paths and fluxes observed within the beach face region of a prototype-scale coastal sand barrier were predominantly controlled by the action of waves at the beach face and resulting runup in-/exfiltration occurring across the swash zone. Regardless of the overall barrier hydraulic gradients, all tests undertaken to complete this study developed a seaward gradient in this zone under the influence of waves (Figures 4 & 6). This outcome, combined with the additional observation of the development of localised groundwater flow divides (Figure 4) in this same region, necessitates a move away from the 'simple' concept that groundwater exchange though coastal sand barriers may be approached by consideration of regional (aquifer-scale) hydraulic gradients alone.

For test series A6 where the sea and lagoon levels were maintained by pumping to be the same, a seaward gradient of 4.45 x 10^{-4} m^3/s was developed by the wave action, from the initial condition of nominally no flux without waves (Table 2). This case also created a landward flux, an order of magnitude lower, towards the lagoon (Table 2). In test series A2 (sea < lagoon level) which initially had a steep seaward gradient prior to the waves being turned on, seaward flux increased by a factor of 1.5 under the influence of wave action at the beach face. Finally for test series A4 where the sea level was above the lagoon level, the action of waves reversed the initially landward flux of 8.70 x 10^{-5} m^3/s, to being seaward at 3.8 x 10^{-4} m^3/s. For this latter case (A4) the landward flux at the lagoon only increased marginally. Importantly, for all three tests the seaward fluxes at the beach face under the influence of wave action were nearly identical (Table 2) and the magnitude or direction of the pre-existing hydraulic gradients had no apparent effect. From this, is it reasonable to now generalise these findings for barriers of similar material, considering that the sand barrier in the experiment is rather narrow from the sea to lagoon (varying between 27 and 37 m, depending on lagoon level) and shallow (an aquitard at 3 m below the sea level provided by the flume floor) compared to most natural and engineered coastal barrier systems. As a result of the narrow barrier width, the relative difference in sea and lagoon levels employed created very steep net through-

barrier hydraulics gradients (A2 = 0.033 m/m and A4 = 0.048 m/m) which are at the very high end of what are realistically encountered in nature. Our experiment can therefore be considered the extreme case and for most natural barriers that are wider or have lower overall hydraulic gradients the conditions created by wave action will similarly entirely dominate the water table, hydraulic gradients and fluxes within the beach face. These experimental observations clearly have implications for how we model these systems, since a large proportion of the infiltrated water returns to the sea rather than migrate through to the back of the barrier.

As previously shown, the water table over-height at the beach face (e.g., Nielsen, 2009) is created by the asymmetry in the instantaneous infiltration-exfiltration (Figure 7), with short-duration high-volume infiltration occurring during the initial phase of an individual swash event coinciding with the greatest swash depths, followed by lower volume exfiltration of longer duration as the swash depth declines. This cyclic process, integrated over many waves (Figure 8), builds up the observed quasi-steady state groundwater mound within the beach face. With a cross-shore transect of PT arrays the total net flux of water into and out of the beach face could be determined; however, this was not practically attainable in the current experiment. Instead the resulting net-fluxes and flow paths were determined from the well and piezometer data. As seen from the piezometer data and inferred flow fields in Figure 6 below the beach face, the wave action activates return flow through the entire depth of the flume (presuming that the bottom 0.5 m between the lower piezometers and the flume floor is activated as well) for all tests (high and low lagoon) with waves. The intention with the beach face piezometers was that they should have encompassed the entire circulation cell, however, this turned out to not be the case and the flux calculations based on the piezometric data under-estimates the total flux through the cell: The horizontal fluxes derived from the piezometers (Table 3) are about an order of magnitude lower than the total fluxes derived from the well data through the control plane at the beach sea interface (Table 2). This indicates that not all the seaward flow is captured within the domain of the piezometers. However, the ratios between the horizontal fluxes determined from the well and piezometer data for all three cases are constant. The most accurate

estimate of the flux in the circulation cell is therefore the horizontal flux derived from the flow nets based on the well data (Figure 4). These fluxes, as reported for conditions with waves in Table 2, correspond to 27 to 38 m^3/d or average Darcy seepage rates of 1.8 to 2.6 m/d. This means that considerable amounts of seawater are circulated through the beach face. As pointed out by Robinson et al. (2007) this can constitute a significant portion of the total groundwater discharge to the sea.

The interaction and circulation of sea and lagoon water bodies has important implications to pore water quality within the beach face. Surface waters (whether salty or fresh) near beaches are typically saturated with dissolved oxygen (DO) due to vigorous equilibration with atmospheric oxygen. So the infiltrating water may have an oxygen content ranging from 7.9 to 11.5 mg/L (in the temperature range of 10 to 30 °C). In addition, the content of particulate and dissolved reactive organic matter (OM) may typically also be relatively high in surface waters (Charbonnier et al., 2013). The influx of DO and OM will typically drive degradation of organic matter in the beach face creating a range of chemical conditions from oxygenated in the upper part of the circulation cell and more anoxic conditions in the deeper and distal parts of the circulation cell. If organic or inorganic contaminants are present in the surface water or in the discharging local groundwater, optimal conditions for degradation of different contaminants may exist in different parts of this localised groundwater circulation cell, depending on the degradation pathways and chemical conditions. An example of a typical contaminant of concern in coastal environments is nitrate (NO_3^-), which can be high in agriculturally contaminated groundwater (Andersen et al., 2007 and Ibánhez et al., 2013). Nitrate can be reduced to harmless N_2(g) by reaction with organic matter, but only at low levels of DO, so this process would only occur in the deeper and oxygen depleted part of the circulation cell. This example illustrates that an integrated understanding of flow, transport and chemical processes is necessary to estimate fluxes of reactive contaminants in the beach face.

This study is to our knowledge the first fully field-scale laboratory experiment to report on the dynamics of the recirculation of surface-groundwater in the vicinity of the beach face at temporal

and spatial scales of relevance to these processes. The observations obtained now allows for an in-depth description of the role of groundwater surface water dynamics in the beach face on sediment dynamics morphological changes (reported elsewhere in this volume). Further, the study allows for a description of the circulation cell that develops due to the surface water infiltration into the upper swash zone which then discharges back to the sea in the lower swash zone, without the confounding factors of heterogeneous sediment distribution, tidal excursions and density effects inherent to natural beaches. An improved understanding of this dynamic circulation of surface water within the beach face has implications for a better description of the cycling and processing of nutrients and contaminants within the beach face.

ACKNOWLEDGEMENTS

The work described in this publication was supported by the European Community's 7th Framework Programme through the grant to the budget of the Integrating Activity HYDRALAB IV, contract no. 261520. The academic lead of the project was Gerd Masselink and the Deltares coordinator was Guido Wolters. The BARDEX II partners would like to thank the Delta Flume staff (Leen, Johan, Piet and Ab) for making the experiment such an enjoyable and successful experience.

REFERENCES

Acworth, R.I., 2007. Measurement of vertical environmental-head profiles in unconfined sand aquifers using a multi-channel manometer board. Hydrogeology journal, 15(7), 1279-1289.

Andersen, M.S., Baron, L., Gudbjerg, J., Chapellier, D., Jakobsen, R., Gregersen, J. and Postma, D., 2007. Nitrate-rich groundwater discharging into a coastal marine environment. Journal of Hydrology, 336, 98-114.

Anschutz, P., Smith, T., Mouret, A., Deborde, J., Bujan, S., Poirier, D., Lecroart, P., 2009. Tidal sands as biogeochemical reactors. Estuarine, Coastal and Shelf Science, 84, 84–90.

Bakhtyar, R., Barry, D.A., and Brovelli, A., 2012. Numerical experiments on interactions between wave motion and variable density coastal aquifers. Coastal Engineering, 60, 95-108.

Bakhtyar, R., Brovelli, A., Barry, D.A., and Li, L., 2011. Wave-induced water table fluctuations, sediment transport and beach profile change: Modeling and comparison with large-scale laboratory experiments. Coastal Engineering, 58, 103-118.

Charbonnier, C., Anschutz, P., Poirier, D., Bujan, S., Lecroart, P., 2013. Aerobic respiration in a high-energy sandy beach. Marine Chemistry 155, 10–21

Kang, H.Y., Nielsen, P., Hanslow, D.J., 1994. Watertable overheight due to wave runup on a sandy beach. 24th International Conference on Coastal Engineering, ASCE, 2115-2124.

Ibánhez, J.S., Leote, C., Rocha, C., 2013. Seasonal enhancement of submarine groundwater discharge (SGD)-derived nitrate loading into the Ria Formosa coastal lagoon assessed by 1-D modeling of benthic NO_3^- profiles. Estuarine, Coastal and Shelf Science 132, 56–64

Masselink, G., Puleo, J.A., 2006. Swash-zone morphodynamics. Continental Shelf Research, 26(5), 661-680.

Masselink, G., Ruju, A., Comnley, D., Turner, I.L., Ruessink, G., Matias, A., Thompson, C., Castelle, B., Wolters, G. Large-Scale Barrier Dynamics Experiment II (BARDEX II): experimental design, instrumentation, test programme and data set. Coastal Engineering (this volume).

Nielsen, P., 1999. Groundwater dynamics and salinity in coastal barriers, Journal of Coastal Research, 15(3), 732-740.

Nielsen, P., 2009. Coastal and estuarine processes. World Scientific, 350p.

Post, V.E.A, von Asmuth, J.R., 2013. Review: Hydraulic head measurements-new technologies, classic pitfalls. Hydrogeology journal, 21(4), 737-750.

Rau, G. C., M. S. Andersen, and Acworth, R. I., 2012, Experimental investigation of the thermal dispersivity term and its significance in the heat transport equation for flow in sediments, Water Resources Research, 48(3), W03511.

Robinson, C., Gibbes, B. and Li, L., 2006. Driving mechanisms for groundwater flow and salt transport in a subterranean estuary. Geophysical Research Letters, 33, L03402, doi:10.1029/2005GL025247

Robinson, C., Li, L., and Prommer, H., 2007. Tide-induced recirculation across the aquifer-ocean interface. Water Resour. Res., 43, W07428, doi:10.1029/2006WR005679.

Sous, D., Lambert, A., Rey, V., Michallet, H., 2013. Swash-groundwater dynamics in a sandy beach laboratory experiment. Coastal Engineering, 80, 122-136.

Turner, I.L., 1998. Monitoring groundwater dynamics in the littoral zone at seasonal, storm, tide and swash frequencies. Coastal Engineering, 35(1-2), 1-16.

Turner, I.L., Masselink, G., 1998. Swash infiltration-exfiltration and sediment transport. Journal of Geophysical Research, 103(C13), 30,813-30,824.

Turner, I.L. and Masselink, G., 2012. Coastal gravel barrier hydrology – observations from a prototype-scale laboratory experiment (BARDEX). Coastal Engineering, 63, 13-22.

Turner, I.L., Coates, B.P. and Acworth, R.I., 1996. The effects of tides and waves to groundwater elevations in coastal zones, Hydrogeology Journal, 4(2), 51-69.

Wakao, N., and S. O. Kagei (1982), Heat and Mass Transfer in Packed Beds, 364 pp., Gordon and Breach, N.Y.

Williams, J., Buscombe, D., Masselink, G., Turner, I.L. and Swinkels, C., 2012. Barrier Dynamics Experiment (BARDEX): Aims, design and procedures. Coastal Engineering, 63, 3-12.

Table 1

Test	*H_s (m)*	*T_p (m)*	*h_s (m)*	*h_l (m)*
A1	0.8	8	3.00	3.00 – 3.40
A2	0.8	8	3.00	4.30
A4	0.8	8	3.00	1.75
A6	0.6	12	3.00	3.00
A7	0.6	12	3.00	4.25
A8	0.6	12	3.00	1.75

Table 2

Series	**Hydraulic Heads**	**Sea control plane without waves [m^3/s]**	**Sea control plane with waves [m^3/s]**	**Lagoon control plane without waves [m^3/s]**	**Lagoon control plane with waves [m^3/s]**
A6	sea = lagoon	-9.38E-05	-4.45E-04	-1.74E-05	4.78E-05
A2	sea < lagoon	-2.05E-04	-3.14E-04	-3.75E-04	-2.58E-04
A4	sea > lagoon	8.70E-05	-3.83E-04	6.46E-05	7.55E-05

Table 3

Series	**Hydraulic Heads**	**Horizontal Flux [$m^3/s/m$]**	**Vertical Flux [$m^3/s/m$]**
A6	sea = lagoon	-3.25E-05	2.98E-06
A2	sea < lagoon	-2.51E-05	1.69E-06
A4	sea > lagoon	-2.92E-05	3.64E-06

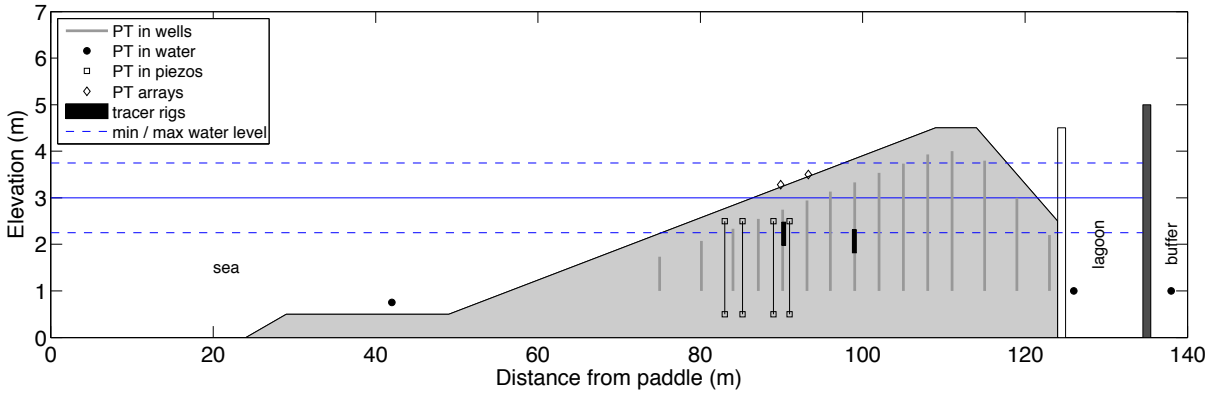

Figure 1

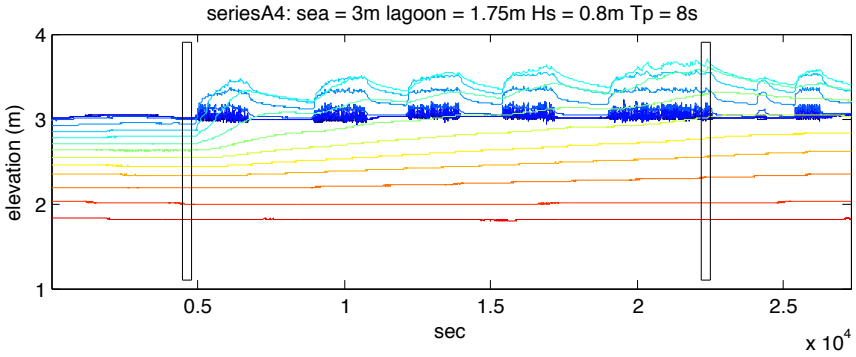

Figure 2

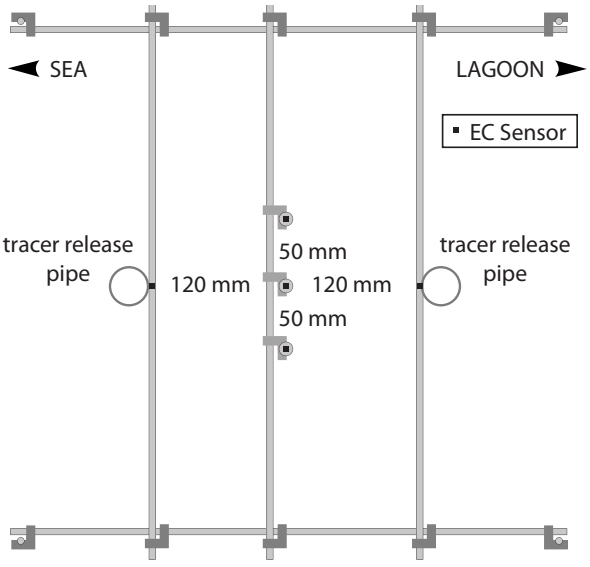

Figure 3

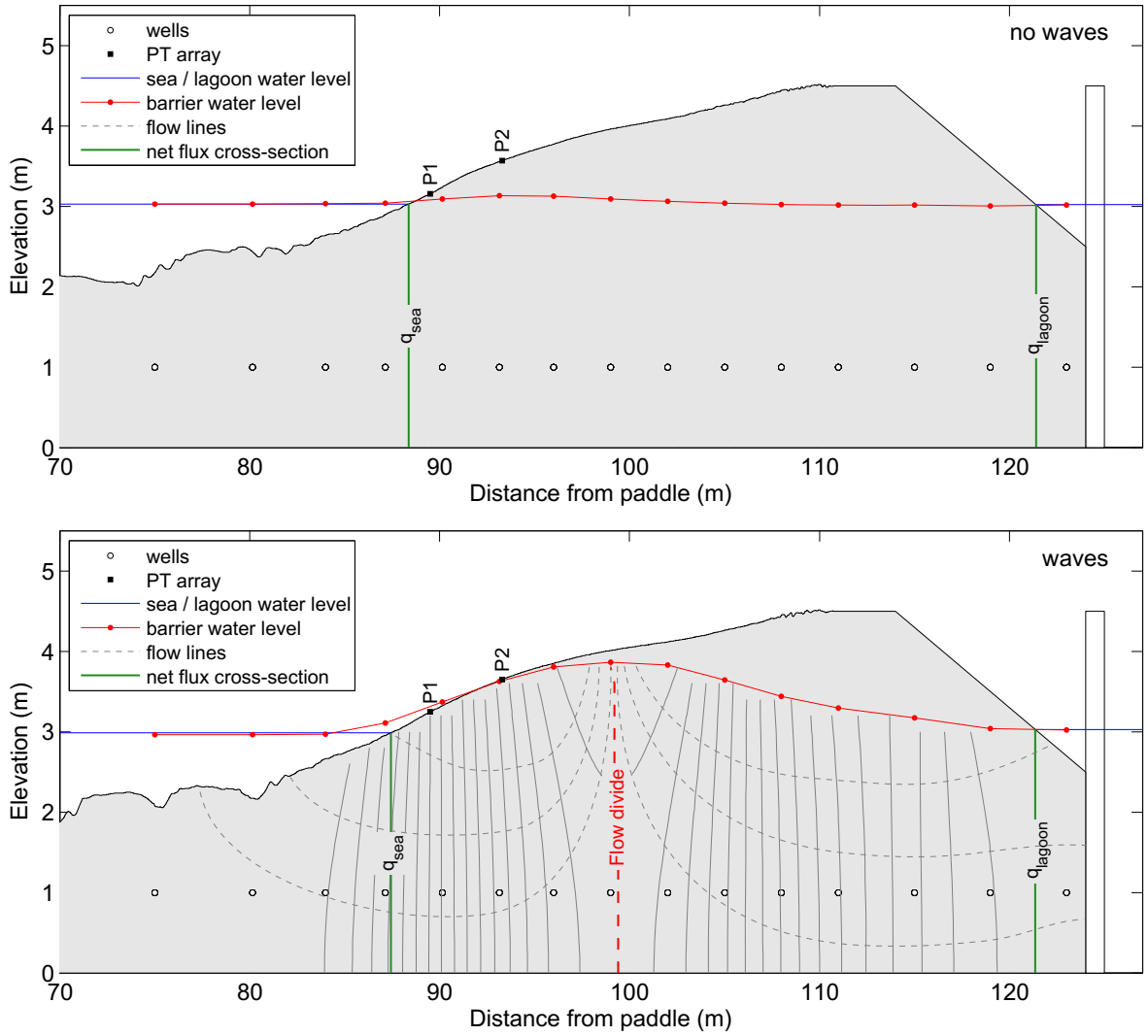
wells
PT array
sea / lagoon water level
barrier water level
flow lines
net flux cross-section
no waves
P1
P2
q_{sea}
q_{lagoon}
Elevation (m)
Distance from paddle (m)
waves
Flow divide

Figure 4a

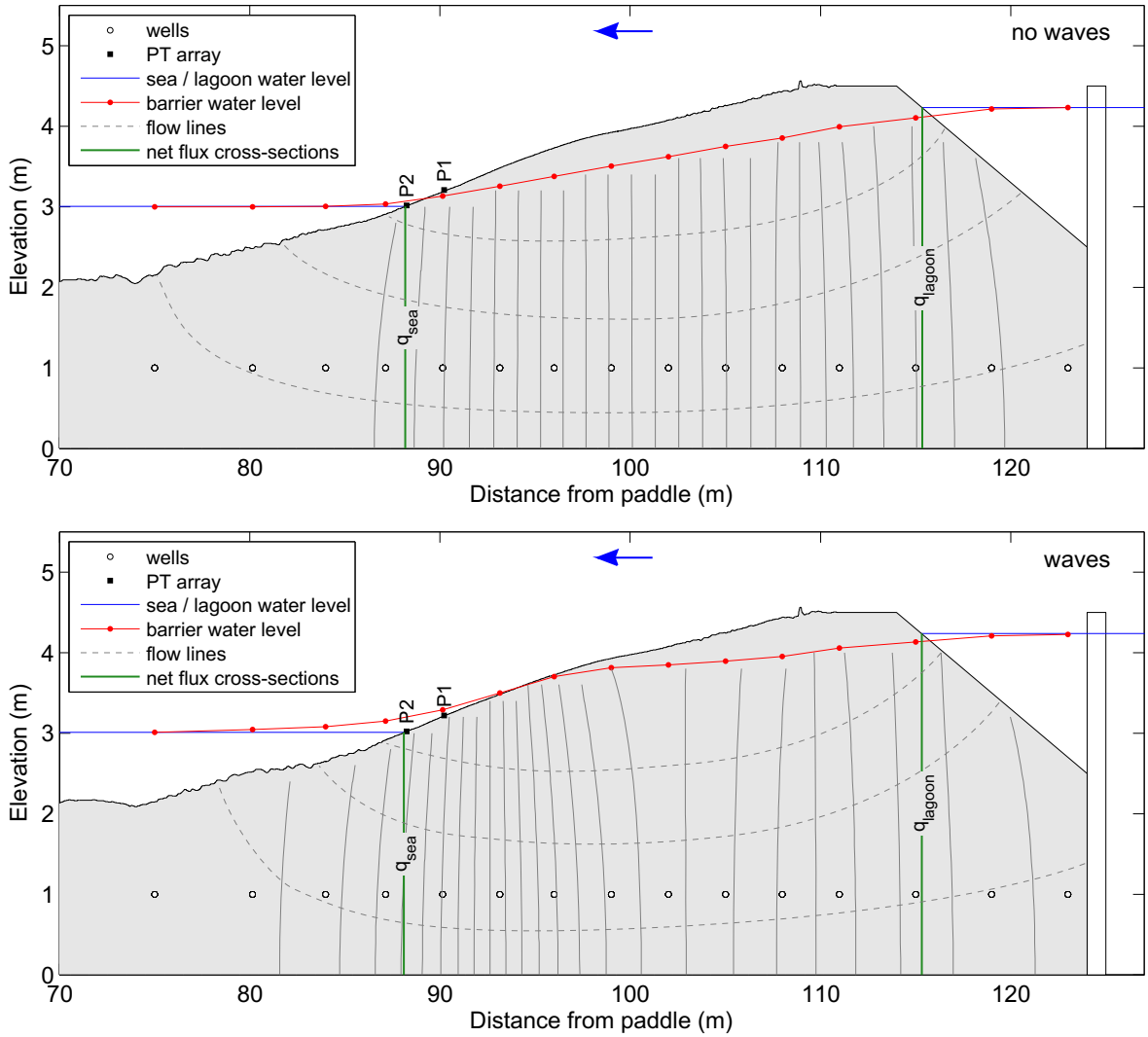
wells
PT array
sea / lagoon water level
barrier water level
flow lines
net flux cross-sections
no waves
P2
P1
q_{sea}
q_{lagoon}
Elevation (m)
Distance from paddle (m)
waves

Figure 4b

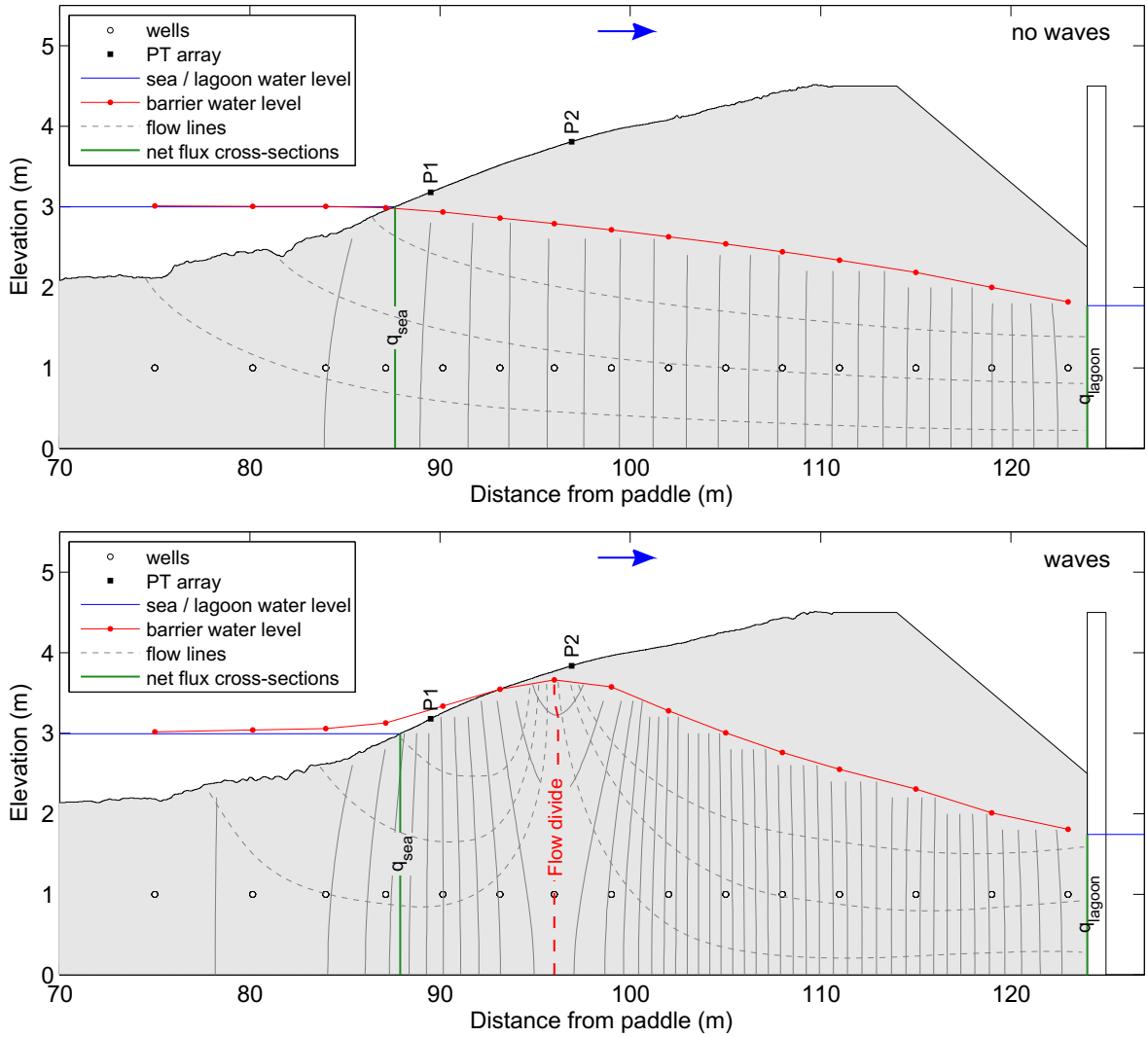
wells
PT array
sea / lagoon water level
barrier water level
flow lines
net flux cross-sections
no waves
P1
P2
q_{sea}
q_{lagoon}
Elevation (m)
Distance from paddle (m)
waves
Flow divide

Figure 4c

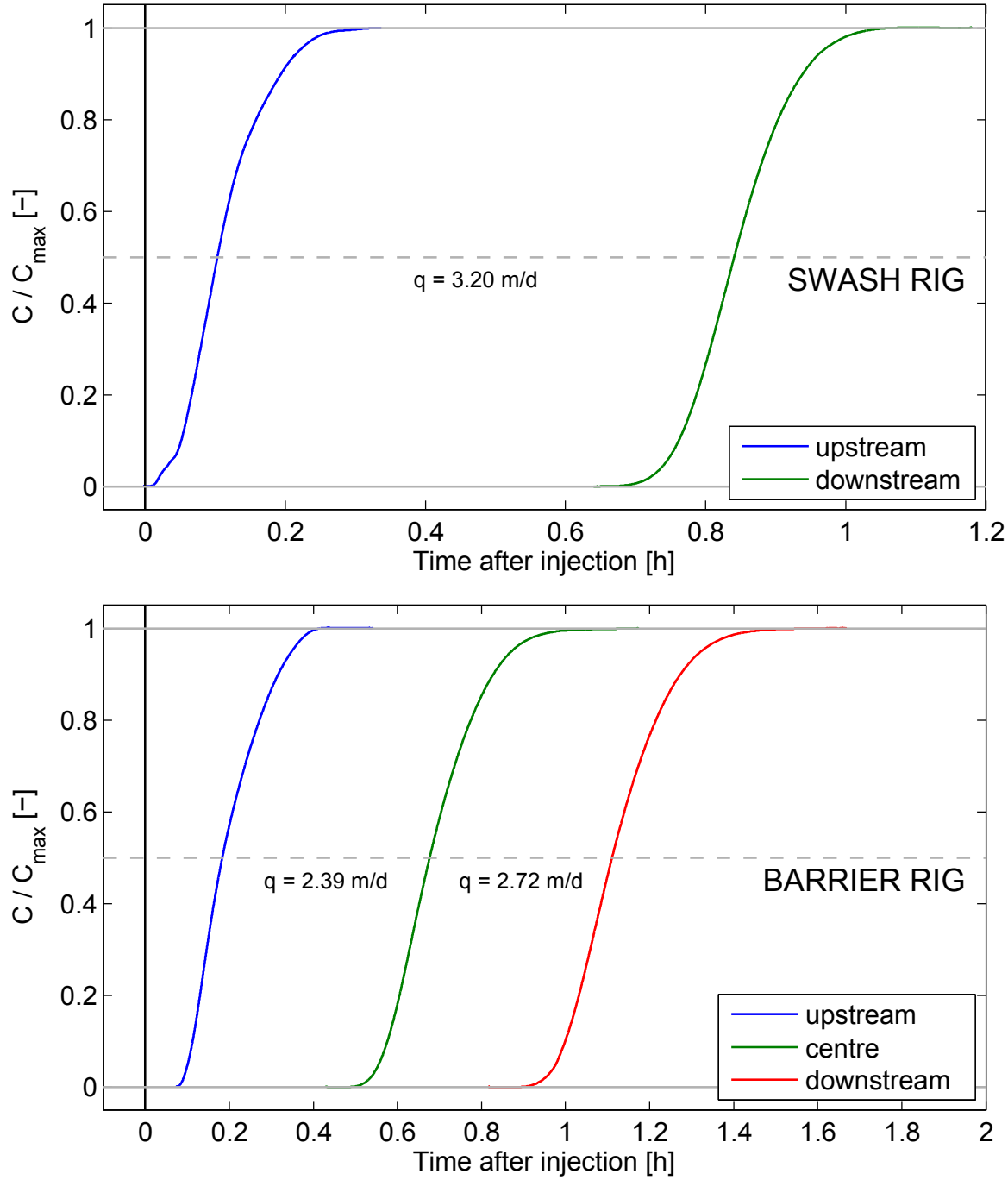
C / C_max [–]
Time after injection [h]
q = 3.20 m/d
SWASH RIG
upstream
downstream
q = 2.39 m/d
q = 2.72 m/d
BARRIER RIG
upstream
centre
downstream

Figure 5

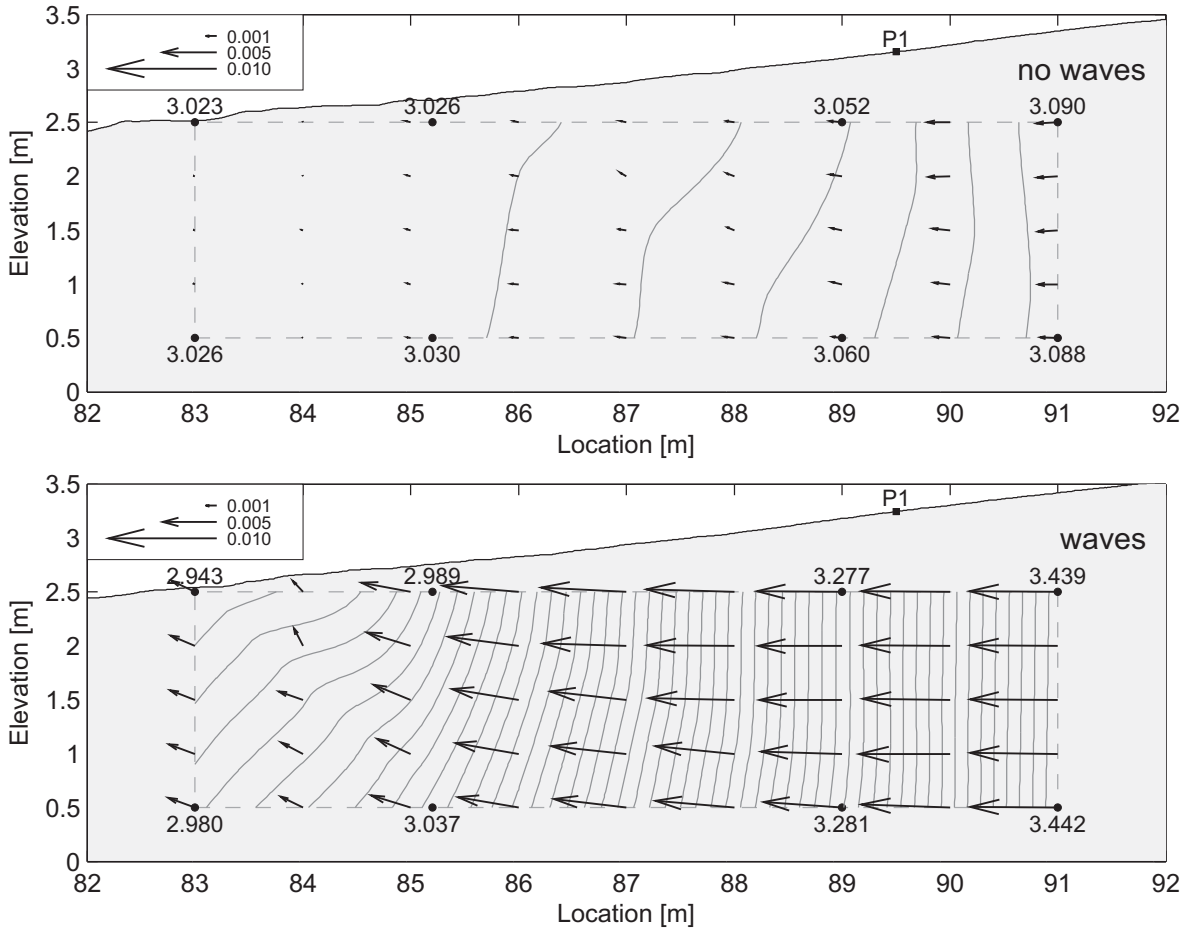
0.001
0.005
0.010
P1
no waves
3.023
3.026
3.052
3.090
3.026
3.030
3.060
3.088
Elevation [m]
Location [m]
0.001
0.005
0.010
P1
waves
2.943
2.989
3.277
3.439
2.980
3.037
3.281
3.442
Elevation [m]
Location [m]

Figure 6a

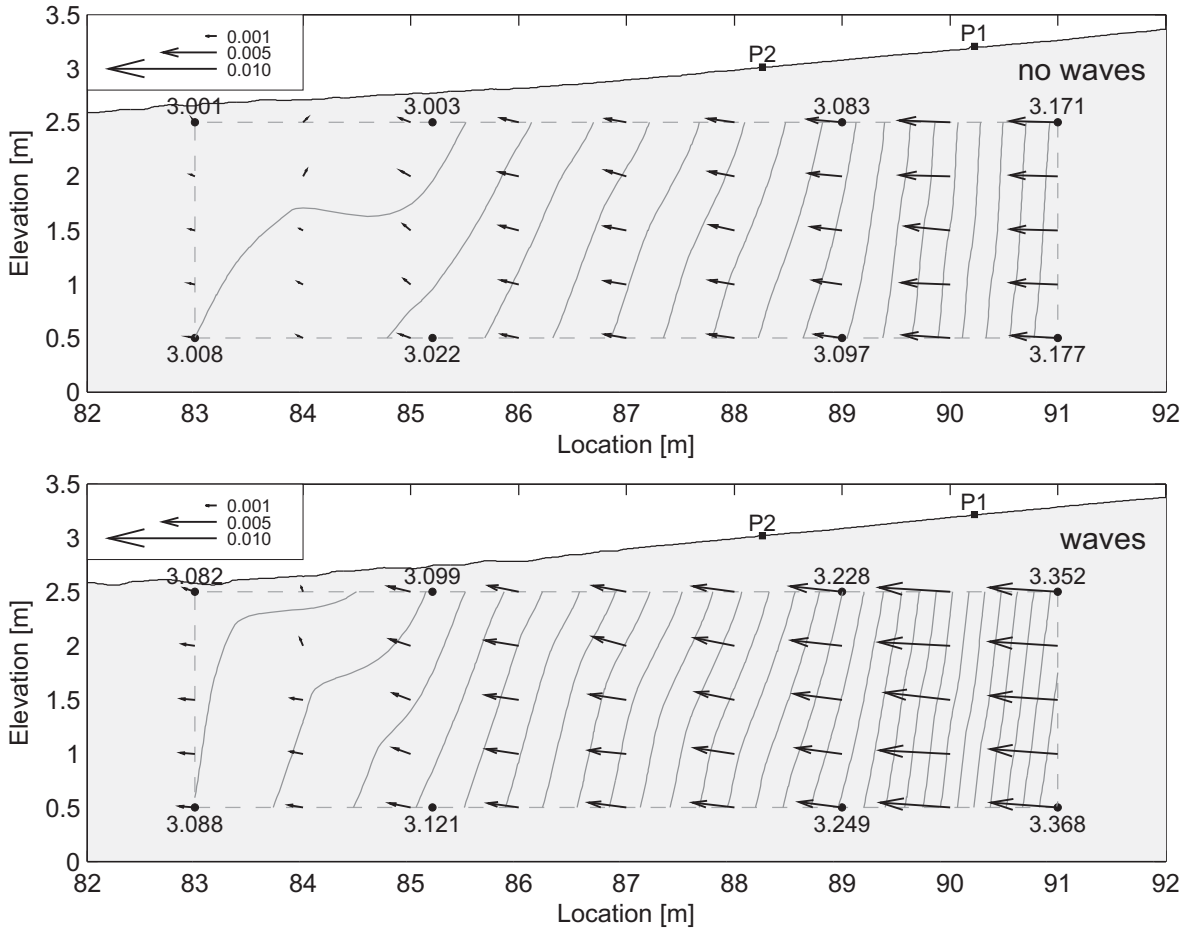
0.001
0.005
0.010
P1
P2
no waves
3.001
3.003
3.083
3.171
3.008
3.022
3.097
3.177
Elevation [m]
Location [m]
0.001
0.005
0.010
P1
P2
waves
3.082
3.099
3.228
3.352
3.088
3.121
3.249
3.368
Elevation [m]
Location [m]

Figure 6b

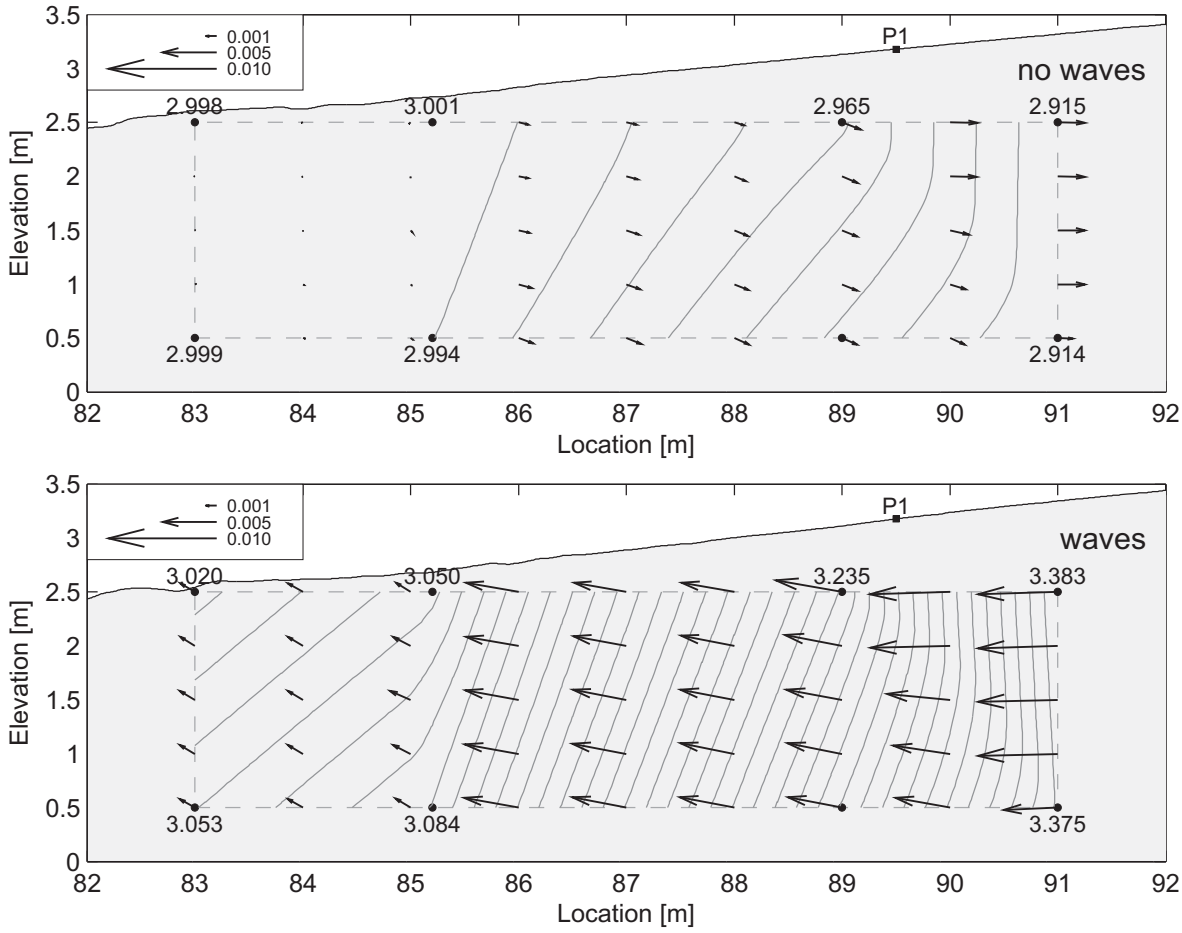
0.001
0.005
0.010
P1
no waves
2.998
3.001
2.965
2.915
2.999
2.994
2.914
Elevation [m]
Location [m]
0.001
0.005
0.010
P1
waves
3.020
3.050
3.235
3.383
3.053
3.084
3.375
Elevation [m]
Location [m]

Figure 6c

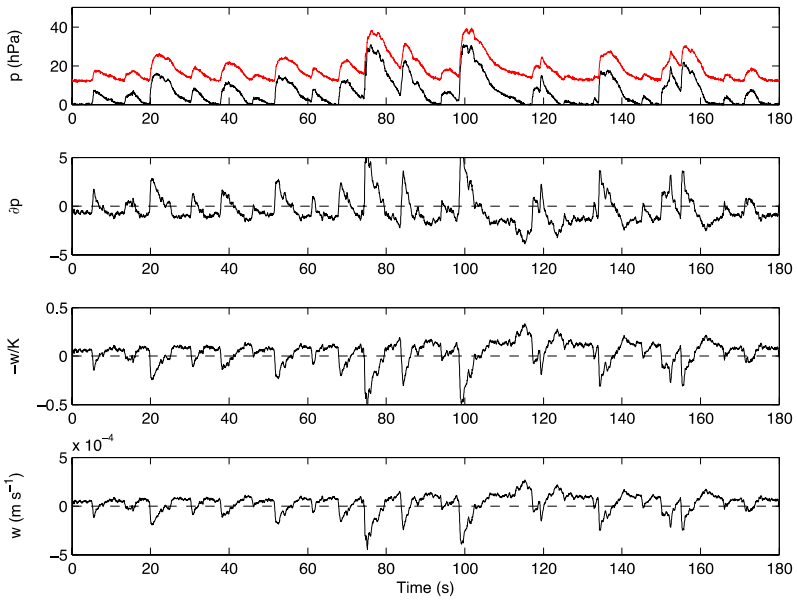

Figure 7a

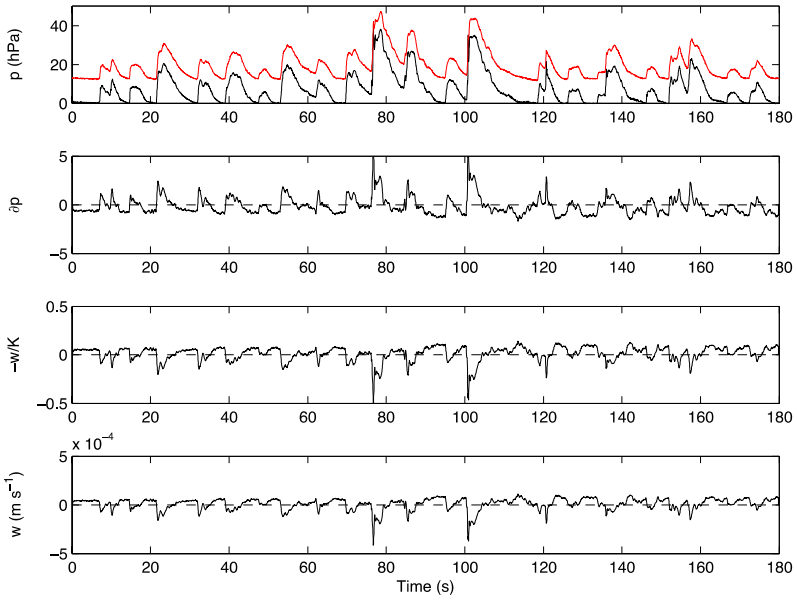

Figure 7b

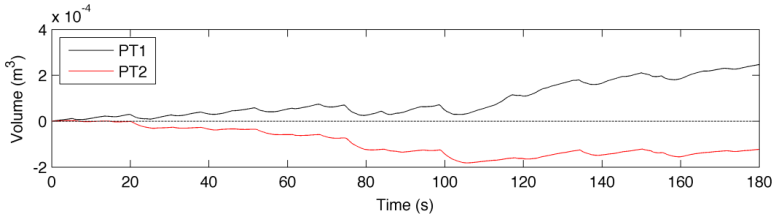

Figure 8

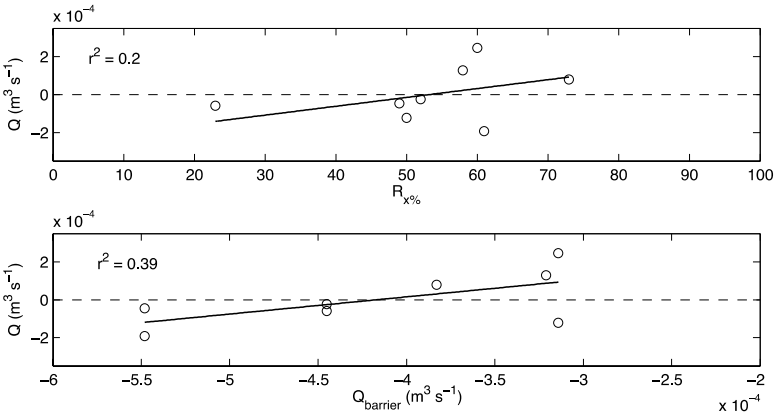

Figure 9